Paper No.
7502

NACE® INTERNATIONAL CORROSION 2016 CONFERENCE & EXPO

The Role of Iron Sulfide Polymorphism in Localized H_2S Corrosion of Mild Steel

Jing Ning, Yougui Zheng, Bruce Brown, David Young, and Srdjan Nesic
Institute for Corrosion and Multiphase Technology, Ohio University
342 West State Street
Athens, OH, 45701
USA

ABSTRACT

Localized corrosion in sour fields is a challenge persisting in the oil and gas industry since it has frequently been seen as a cause for catastrophic failures of upstream pipelines. Hence, prediction and mitigation of H_2S localized corrosion of mild steel is of key importance for integrity management. However, our current understanding of H_2S localized corrosion mechanism(s) from numerous studies in both in the laboratory and the field is far from being conclusive. Especially, the environmental conditions that may cause localized H_2S corrosion are unclear. Therefore, defining an experimental condition in the laboratory that can replicate localized corrosion in a sour environment is critical to our understanding of mechanisms of localized corrosion. The focus of the present research was to explore environmental conditions leading to localized H_2S corrosion. It was found that severe localized corrosion was repeatedly observed in experiments, when there was a simultaneous formation of greigite and/or pyrite. Based on those experimental results, a hypothesis for a mechanism of H_2S localized corrosion was proposed.

Keywords: *Hydrogen sulfide, localized corrosion, iron sulfide, polymorphism*

INTRODUCTION

Corrosion caused by the presence of H_2S and CO_2 in produced fluids is frequently encountered in pipelines during the production of oil and gas. Compared to general CO_2 and H_2S corrosion[1-3], localized H_2S corrosion is much less understood and less studied. This poses a key challenge for integrity management in the oil and gas industry.

In open literature, H_2S localized corrosion has been usually associated with multiple risk factors, such as the presence of elemental sulfur[4-8], the presence of polysulfides[9-11], high salinity[12-14], flow velocity[15], a change in local water chemistry at steel surface[16], and metallurgy. In addition, corrosion and scaling mitigation strategies, such as corrosion inhibitors, alcohol and glycols, and pH stabilization, used in sour systems in the oil and gas industry, can greatly decrease the uniform corrosion, while increasing the probability for localized corrosion. Kvarekval *et al.*[17] have showed very strong evidence of this with examples of severe localized corrosion.

Moreover, numerous studies[1, 2, 18-21] have revealed that formation of an iron sulfide layer on the steel surface usually can suppress uniform corrosion, which is related to this layer acting as a diffusion

barrier and by surface blockage effect. In those studies, mackinawite was observed as the dominant iron sulfide phase. In fact, polymorphous iron sulfides have been reported as corrosion products in sour oil and gas fields[23-25] and in laboratory experiments[1, 26-28]. A few studies[30-33] have been conducted to explore the impact of different iron sulfide phases on the corrosion process in sour environments. In these studies, severe localized corrosion has been reported in the presence of a mackinawite deposit layer[30,32,33], but not in the presence of pyrrhotite and troilite[30,31]. Therefore, in the present study, the focus was on further investigation of localized corrosion seen in a sour environment and the possible link with iron sulfide polymorphism.

EXPERIMENTAL

Experimental Methodology

A thermodynamic model[35] (in the form of Pourbaix diagrams) was used to design experimental conditions leading to formation of different iron sulfides as corrosion products in a sour environment. The subsequent influence of a corrosion product layer containing polymorphous iron sulfides on the corrosion process of steel with focus on localized corrosion was studied. Three sets of experiments were designed and executed as described below:

Experimental set #1: Experiments with spontaneous formation of polymorphous iron sulfides (mackinawite, pyrrhotite, greigite, and pyrite) were designed and conducted at 80 ^{o}C, where formation of polymorphous iron sulfides would be facilitated by a relatively high temperature.

Experimental set #2: Experiments with formation of greigite and pyrite triggered by changing the solution pH was designed and carried out at 25 ^{o}C. At these experimental conditions, only mackinawite and pyrrhotite were allowed to form for one week before the solution pH was changed to facilitate formation of greigite and/or pyrite on the basis of predictions made by Pourbaix diagrams.

Experimental set #3: Experiments similar to those in set #2 except that the change of solution pH was done after 2 days before a significant mackinawite/pyrrhotite layer formed, which is considered to be precursors to transformation into more thermodynamically stable iron sulfides such as greigite and pyrite.

Apparatus

The experimental setup is shown in Figure 1. Experiments were performed in a 2-liter glass cell filled with 1 *wt.* % sodium chloride (NaCl) electrolyte. Each experiment contained six to ten square shaped steel specimens with dimensions of 1.2 cm x 1.2 cm x 0.2 cm, hung in the glass cell using nylon string, and one cylindrical working electrode (WE) specimen with dimensions of 1.2 cm diameter x 1.5 cm length, mounted on a stationary rod, with the total volume/area ration being 0.075 cm. The square specimens were used for surface analysis and weight loss measurements, while the stationary WE was used for electrochemical measurements. A magnetic stir bar was used to keep the solution fully mixed during the experiments. A typical 3-electrode setup was used to conduct electrochemical measurements. A platinum wire was used as the counter electrode. A saturated silver-silver chloride (Ag / AgCl) electrode connected to the cell externally through a Luggin capillary was used as the reference electrode. The theoretical B value used in linear polarization resistance (LPR) measurements was adjusted using weight loss results, and was found to be 13 mV/decade on average in this study. A mesh capped pH probe[34] was used to measure surface pH at a corroding surface and a glass pH probe was used to monitor bulk solution pH.

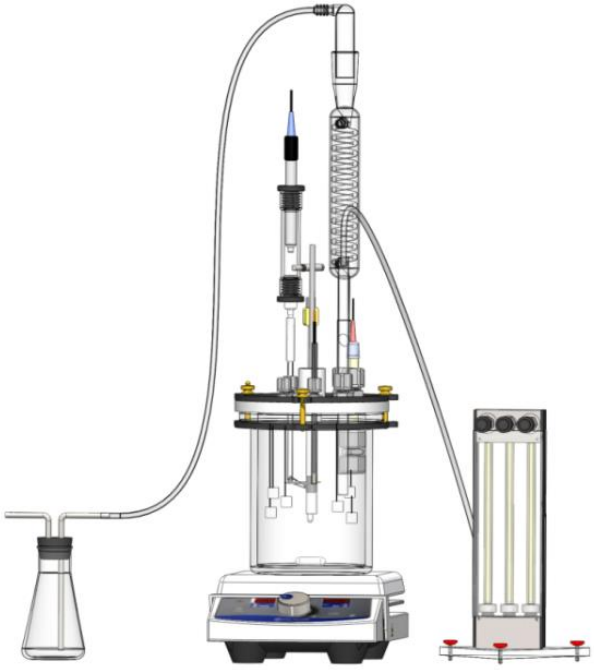

Figure 1. Experimental setup.

Material

The test specimens were all made from API[(1)] 5L X65 carbon steel. The chemical composition of this carbon steel is shown in Table 1.

Table 1 Chemical composition of 5L X65 carbon steel used in experiment (*wt.* %).

Cr	Mo	S	V	Si	C	Fe	Ni	Mn	P
0.14	0.16	0.009	0.047	0.26	0.13	Balance	0.36	1.16	0.009

Procedure

The test conditions for this series of experiments are shown in Table 2. In the beginning of each test, N_2 gas was sparged through the electrolyte to deoxygenate the solution (typically more than 4 hours). An H_2S and N_2 pre-mixed gas was then sparged into the solution continuously throughout the experiment. The solution pH, decreased due to the addition of H_2S to the solution, and was adjusted to 6.0 by using a deoxygenated 1.0 M NaOH solution. The specimens were polished to a 600 grit sandpaper finish, rinsed thoroughly with deionized water and isopropanol, ultrasonically cleaned in isopropanol, and dried by an air blower before immersion in electrolyte. Experiments were conducted following the experimental designs shown in Figure 2, Figure 3, and Figure 4, which indicate the specimen removal times with specific analysis designations for each. Solution pH was adjusted to 11.5 after 7 days of exposure in Exp. set #2 as indicated in Figure 3 and after 2 days of exposure in Exp. set #3 as indicated in Figure 4. In both cases the pH spontaneously decreased to pH 7.0 very quickly. While taking special care that oxygen ingress was prevented, corroded square specimens were taken out for analysis on the days indicated in the timeline, rinsed with deoxygenated DI water and deoxygenated isopropanol, blown dry using N_2, and stored in a desiccator. Scanning electron microscope (SEM) imaging was used to detect the surface morphology of the specimens, energy dispersive X-ray spectrometry (EDX) and X-ray diffraction (XRD) was applied to determine the nature of iron sulfide formed on the specimens. Solution was drawn from the glass cell immediately before taking each steel specimen, filtered by using a 0.22 µm syringe filter to remove any iron sulfide precipitate from solution, and then measured for ferrous ion concentration using a spectrophotometric method. Bulk pH, surface

[(1)] American Petroleum Institute (API), 1220 L Street, NW, Washington, DC 20005-4070

pH, and open circuit potential (OCP) were monitored throughout the experiment. Both LPR and weight loss (WL) methods were used to obtain corrosion rate measurements.

Table 2 Test matrix.

Description	Exp. #1	Exp. #2	Exp. #3
Temperature	80 °C	25 °C	25 °C
Electrolyte	1 *wt.*% NaCl brine		
Gas composition	10 % H_2S / balance N_2		
H_2S partial pressure	0.053 bar	0.097 bar	0.097 bar
Stirring speed	400 rpm		
Material	API 5L X65		
Initial pH	6.0		

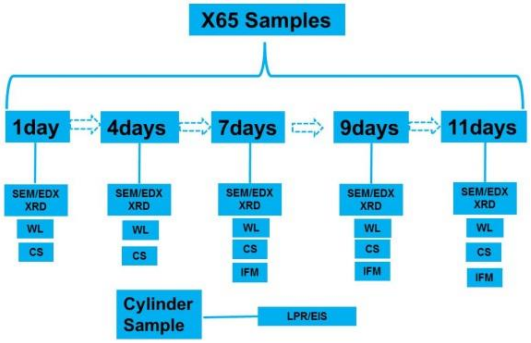

Figure 2. Experimental design for experiment #1.

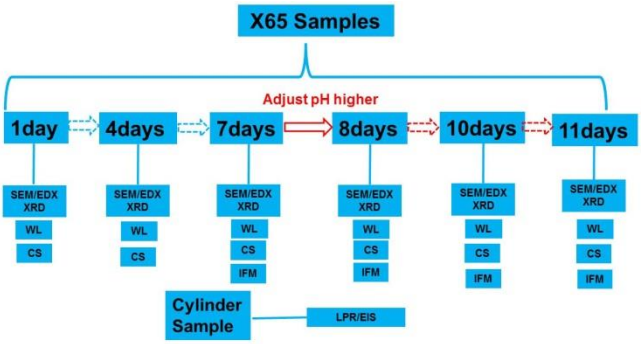

Figure 3. Experimental design for experiment #2.

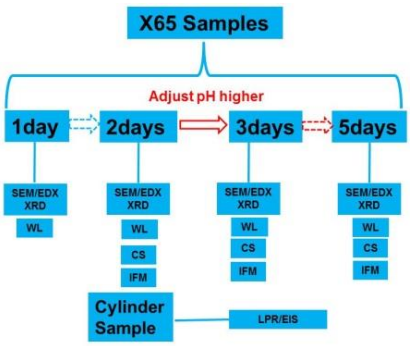

Figure 4. Experimental design for experiment #3.

EXPERIMENTAL RESULTS

Experimental Set #1: Reproducible Occurrence of Localized Corrosion with Spontaneous Formation of Polymorphous Iron Sulfides

Corrosion Behavior

Figure 5 shows OCP, corrosion rate, solution pH, and ferrous ion concentration evolution monitored during the experiments. Corrosion rates obtained from LPR measurements on the WE were verified by weight loss results from the square specimens. The corrosion rate was 1.1 mm/year initially and then decreased to around 0.07 mm/year in the first four days, due to the formation of a protective iron sulfide layer at steel sample surface. However, an increase in both OCP and corrosion rate (with the exception of the high initial values) was observed after four days of exposure, which could be explained by an increase in cathodic reaction rate, but the cause of this was yet unknown. It was hypothesized that this increase in cathodic reaction rate was due to either the collapse of the protective corrosion product layer increasing transport of corrosive species required for cathodic reactions or the formation of conductive corrosion products increasing the overall cathodic reaction area.

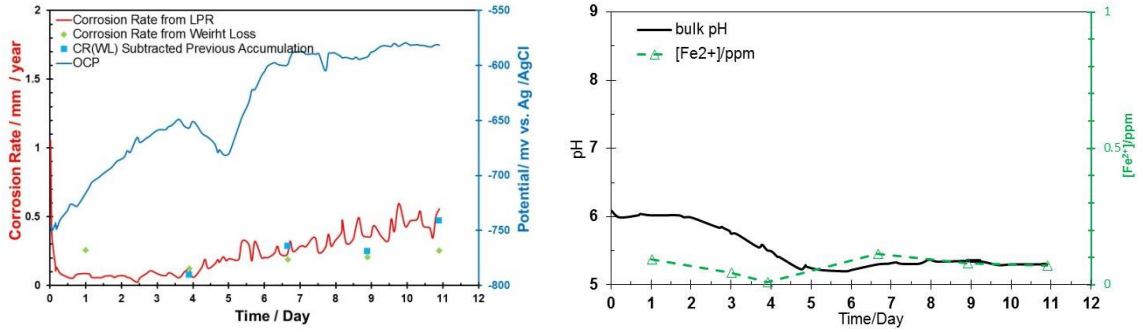

(a) (b)

Figure 5. Parameters monitored throughout Exp. #1 (a) OCP and corrosion rate; (b) Bulk pH and $[Fe^{2+}]$.

Corrosion Products

Figure 6 presents surface morphologies of the square specimens as removed in chronological order. A uniform surface morphology was observed after 1 day and 4 days of exposure, while blistering, cracking, and spalling morphologies were seen after 7 days, 9 days, and 11 days of the experiment.

Table 3 summarizes the XRD quantitative analysis of corrosion products determined by the reference intensity ratio (RIR) methodology in order to better understand formation and transformation of polymorphous iron sulfide phases throughout the experiment. This table clearly shows a transformation of the initial thermodynamically metastable mackinawite to the more stable pyrrhotite and pyrite phases. Mackinawite accounts for 90% of corrosion products formed after 1 day of exposure, while decreasing significantly over exposure duration. In contrast, both pyrrhotite and pyrite phases have a dramatic increase throughout the experiment. In addition, the formation of greigite was indicated as a corrosion product after 1 day through 9 days of exposure, but was not observed on the last sample from the experiment. That is because greigite is also a metastable phase, developed from the initial mackinawite and then transformed completely to the final thermodynamically stable pyrite after 11 days.

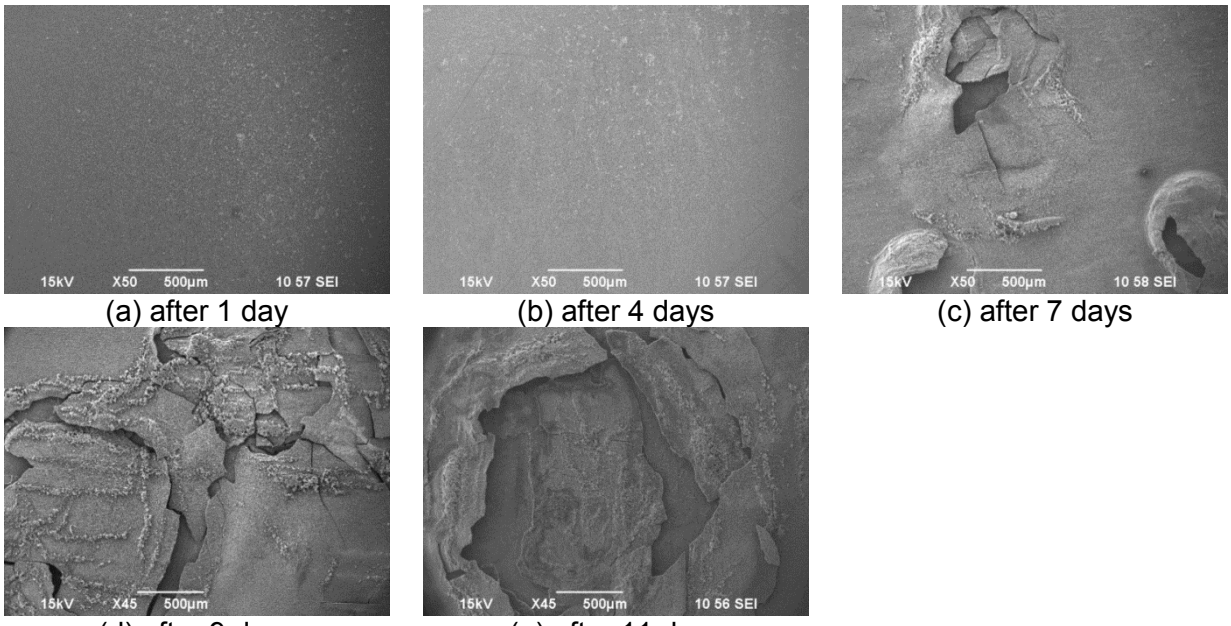

(a) after 1 day (b) after 4 days (c) after 7 days

(d) after 9 days (e) after 11 days

Figure 6. Surface morphologies of samples: (a) after 1 day; (b) after 4 days; (c) after 7 days; (d) after 9 days; (e) after 11 days.

Table 3 XRD quantitative analysis of corrosion products formed in experiment #1.

Phases	1 day	4 days	7 days	9 days	11 days
Mackinawite	90.0 %	76.4 %	49.2 %	63.6 %	66.0 %
Pyrrhotite	8.0 %	5.8 %	14.8 %	1.9 %	16.4 %
Greigite	2.0 %	2.2 %	3.3 %	3.3 %	0
Pyrite	0	4.8 %	27.8 %	18.5 %	10.6 %
Iron Carbide	0	10.8 %	4.9 %	12.7 %	7.0 %

To have a closer look at the corrosion product layer, surface morphology and cross section SEM images of samples after 4 days and after 7 days, at a higher magnification, are shown in Figure 7. A lot of small cubic crystals were observed on the mackinawite layer in the surface SEM images of samples shown in (a) and (b), which are believed to be pyrite crystals on the basis of XRD findings. Further, cross section images presented in (c) and (d) are backscattered electron composition (BEC) images which show atomic differences by changes of contrast in the image. In general, darker areas that appear in BEC images are atomically lighter while brighter areas are atomically heavier. Accordingly, the crystals with lighter color on top of the grey mackinawite layer are considered to be pyrite as seen on the surface SEM images (a) and (b). Note that there are many crystals with the lighter color embedded in the darker mackinawite layers of the cross section sample, suggesting that pyrite crystals are also embedded in the mackinawite layer. Furthermore, a steady increase in the thickness of the iron sulfide layer formed on steel surface throughout experiment was observed. Hence, the first hypothesis proposed for the increase in both OCP and corrosion rate when there was initiation of localized corrosion, a loss of diffusion barrier layer increasing the transport of corrosive species, is proven to be wrong. Therefore, the second hypothesis, the formation of a conductive corrosion product layer increasing overall cathodic reaction area, was taken into consideration.

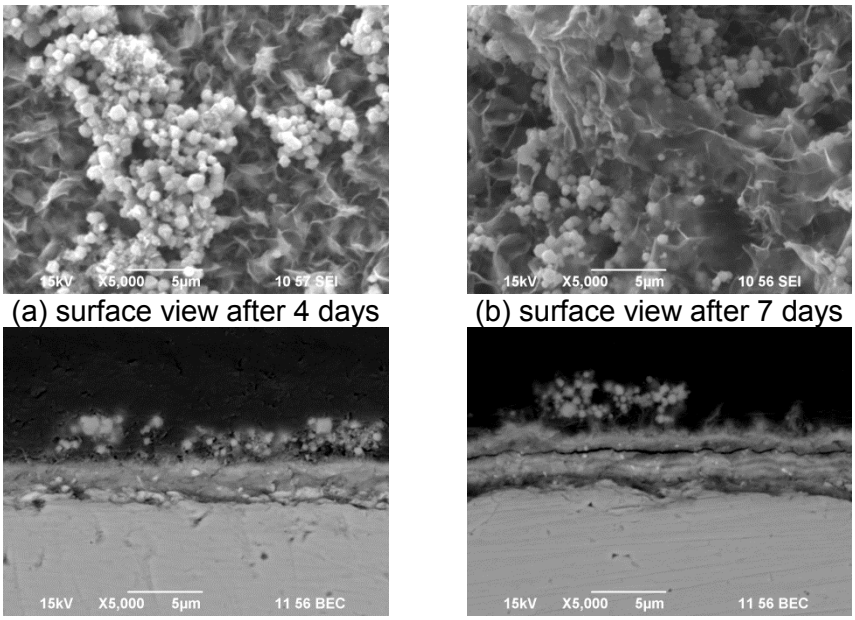

(a) surface view after 4 days (b) surface view after 7 days

(c) cross section after 4 days (d) cross section after 7 days

Figure 7. SEM images with x 5, 000 magnification: (a) surface view after 4 days; (b) surface view after 7 days; (c) cross section after 4 days; (d) cross section after 7 days.

Surface Profilometry of Samples after Removing Corrosion Product Layer

The corrosion product layer was removed by using a Clarke solution[36] and a cleaning method as outlined in ASTM G1[37] to observe the corroded steel underneath. A flat surface owing to uniform corrosion after 4 days of test was seen in Figure 8 (a). Then, initiation of localized corrosion was observed as 10 µm deep pits after 7 days in Figure 8 (b). And finally, propagation of localized corrosion can be observed in Figure 8 (c) and (d). At the end of this experiment, after 11 days of exposure, a 40 µm depth of localized corrosion was measured. The penetration rate based on this 40 µm depth was calculated to be 2.1 mm/year. As compared to the general corrosion rate in the initial 4 days of 0.07 mm/year, significant localized corrosion occurred. It should be noted that the localized corrosion occurred when quantitative analysis shows higher concentrations of greigite and/or pyrite in the corrosion product, which indicates a probable correlation between localized corrosion and the formation of greigite and/or pyrite. This hypothesis was further verified in the following experiments.

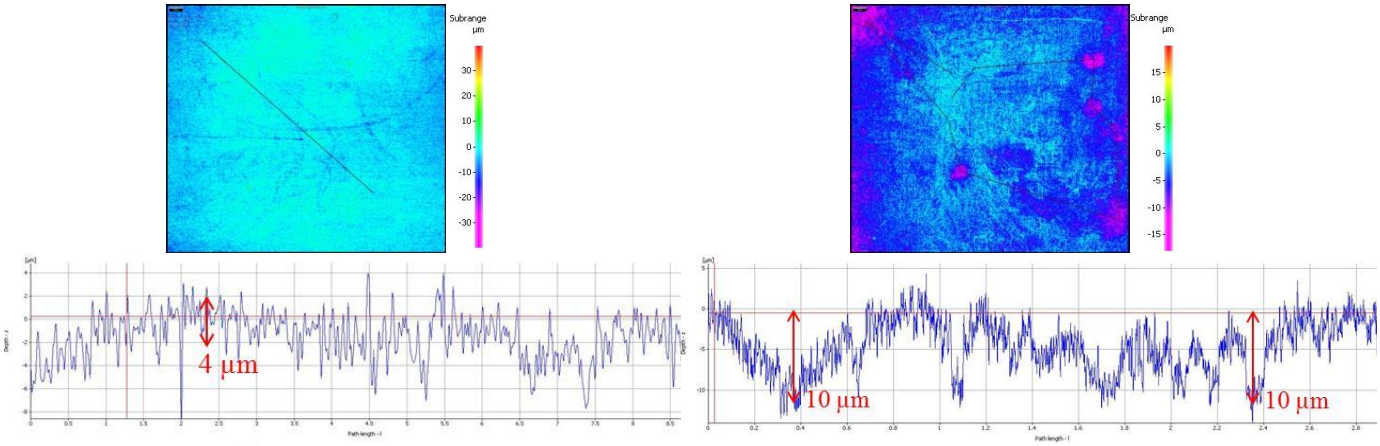

(a) after 4 days (b) after 7 days

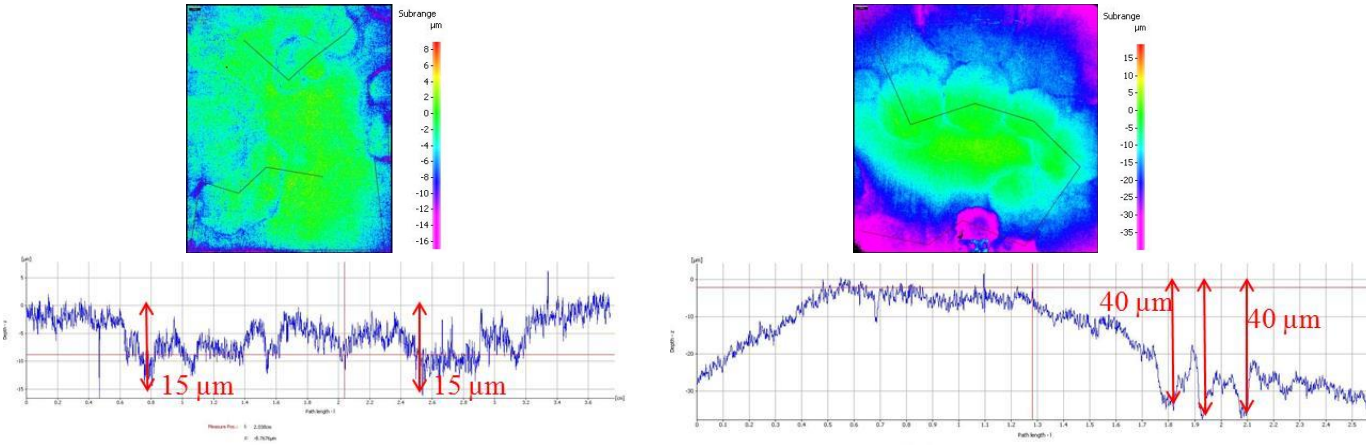

(c) after 9 days (d) after 11 days

Figure 8. Surface profilometry of samples after removing corrosion product layer: (a) after 4 days; (b) after 7 days; (c) after 9 days; (d) after 11 days.

Experimental set #2: Localized Corrosion Triggered by Facilitating Formation of Greigite/Pyrite at Low Temperature

Experimental set #1 indicated a probable correlation between localized corrosion and the formation of greigite and/or pyrite. To further verify this hypothesis, the Experimental set #2 was designed and carried out at 25 °C by adjusting solution pH after 7 days of exposure to trigger greigite and/or pyrite formation according to Pourbaix diagrams. Figure 9 shows Pourbaix diagrams generated at the experimental conditions after 7 days of exposure, and, accordingly, greigite and/or pyrite are expected to form if the solution pH is adjusted from a low value (around pH 5) to a high value (above pH 11).

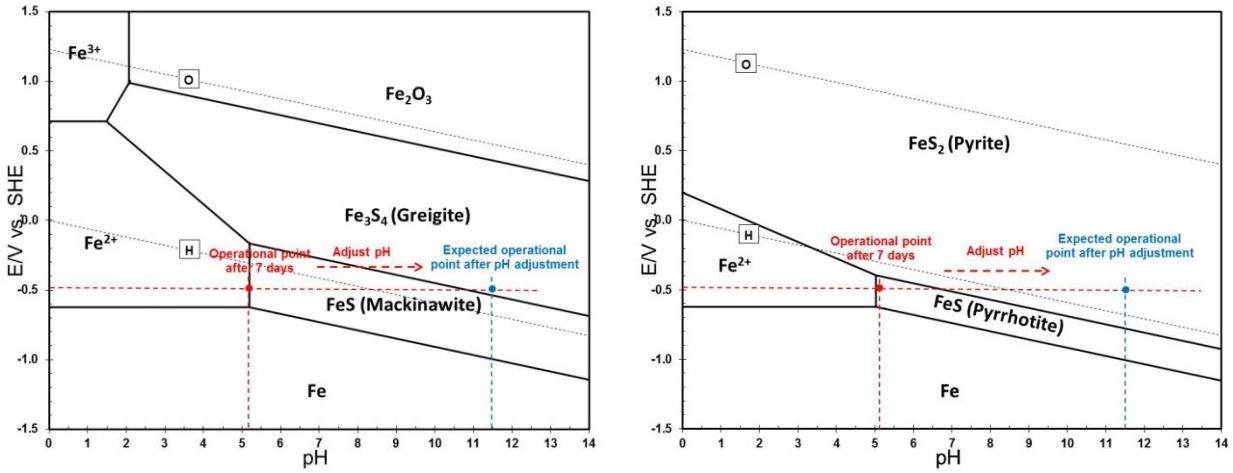

(a) Mackinawite / Greigite (b) Mackinawite / Greigite / Pyrrhotite / Pyrite

Figure 9. Thermodynamic considerations for the formation of iron sulfides triggered by adjusting pH at 25 °C according to Pourbaix diagram predictions: (a) only mackinawite/greigite considered; (b) all expected iron sulfides considered.

Corrosion Behavior

Figure 10 (a) shows bulk pH and surface pH monitored during this experiment. As mentioned above, solution pH was adjusted from pH 5.5 to 11.5 after 7 days of exposure using deoxygenated NaOH solution, but quickly decreased spontaneously to approximately pH 7.0. Figure 10 (b) shows the OCP and corrosion rates throughout the experiment. Both corrosion rates and OCP were very stable throughout the initial seven days of experiment, but did have a significant increase immediately after adjusting the solution pH and kept slowly increasing until the end of the experiment. In addition, weight loss was also carried out confirming LPR measurements. It is noteworthy that weight loss results were

corrected by subtracting from previous accumulation in order to properly compare them with LPR measurements.

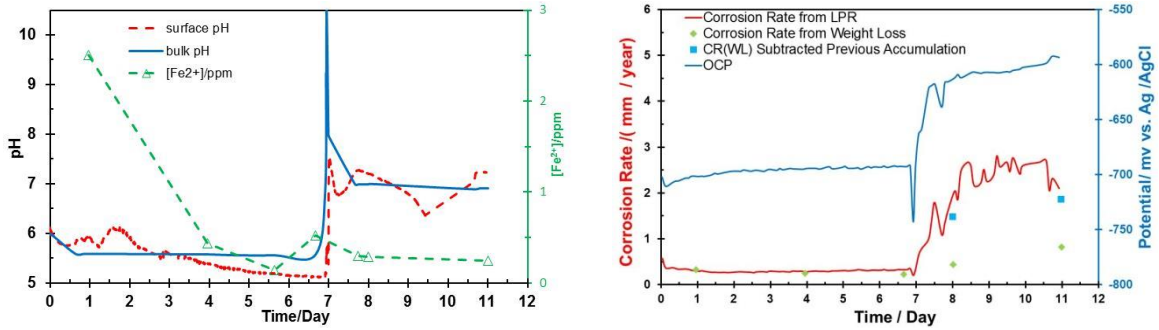

(a) (b)

Figure 10. Parameters monitored throughout Experiment #2: (a) bulk pH, surface pH, and [Fe^{2+}]; (b) corrosion rates and OCP.

Corrosion Products

Table 4 shows the quantitative analysis of corrosion products formed on samples during this experiment. The formation of greigite after adjustment of solution pH is obvious as the percentage of the greigite phase changes from zero before pH adjustment to 9.0 % after the pH adjustment and to 17.9 % after the 11th day of the experiment. Pyrite was also observed on the last sample. In addition, a decrease in the mackinawite phase can be observed from 90.8 % after 7 days to 78.6 % after 11 days.

Table 4 XRD quantitative analysis of corrosion products formed in experiment #2.

Phases	7 days	8 days	11 days
Mackinawite	90.8 %	90.4 %	78.6 %
Pyrrhotite	5.2 %	0.3 %	0
Greigite	0	9.0 %	17.9 %
Pyrite	0	0	3.2 %
Iron Carbide	4.0 %	0.3 %	0.3 %

Figure 11 presents the comparison of surface morphologies of samples from Experiment #2. A uniform corrosion product layer was observed on samples in advance of the pH adjustment as shown in Figure 11 (a), (b), and (c). However, spalling and exfoliation of a corrosion product layer can be seen on samples after the adjustment of solution pH shown in Figure 11 (d), (e), and (f).

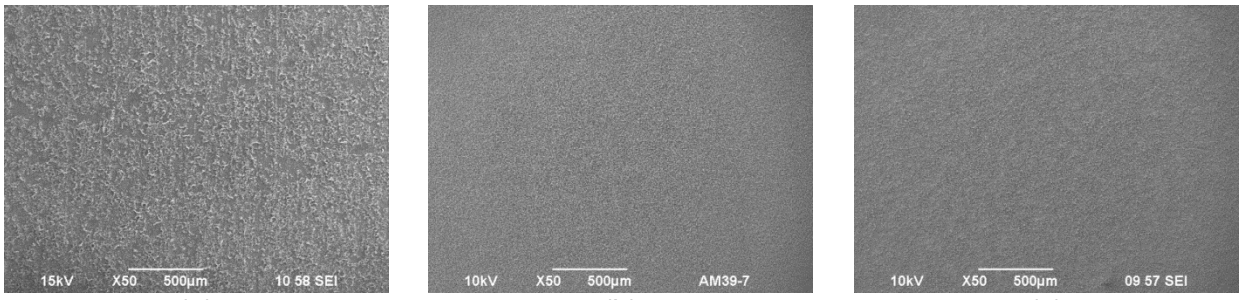

(a) (b) (c)

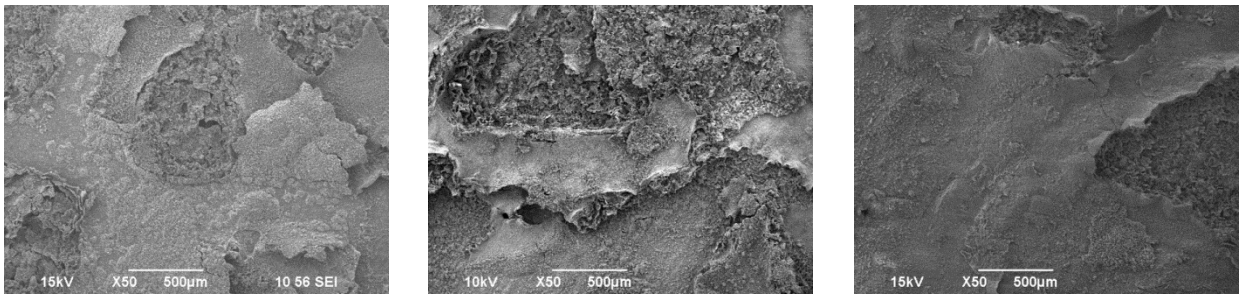

(d) (e) (f)

Figure 11. Surface morphologies of samples in chronological order: (a) after 1 day; (b) after 4 days; (c) after 7 days; (d) after 8 days; (e) after 10 days; (f) after 11 days.

Surface Profilometry of Samples after Removing Corrosion Product Layer

Figure 12 shows surface profilometry of samples after removing the iron sulfide layer. The sample before pH adjustment shown in (a) presents a flat surface due to a 0.3 mm/year general corrosion rate; in contrast, the sample after adjusting pH in (b) shows a locally corroded surface with a 14.6 mm/year pit penetration rate (assuming this localized corrosion occurred in one day). Again, significant localized corrosion was clearly observed when there was a high content of greigite and/or pyrite phases. In addition, an increase in both OCP and corrosion rate was observed again when localized corrosion occurred. This experiment was repeated and the experimental results were reproducible. After the pH adjustment, a dramatic increase in both OCP and corrosion rate was observed, both greigite and pyrite as new corrosion product phases were detected, and severe localized corrosion occurred with approximately the same penetration rate.

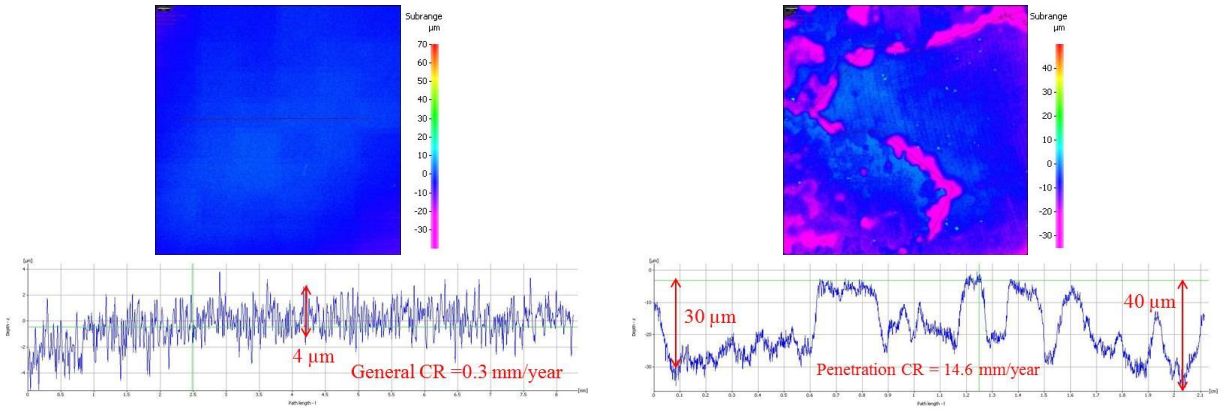

(a) before pH adjustment (b) after pH adjustment

Figure 12. Surface profilometry of samples after removing corrosion product layer: (a) after 7 days; (b) after 8 days.

Experimental set #3: Adjusting Solution pH prior to Formation of Greigite/Pyrite

Experimental set #2 provided strong evidence that there is a correlation between the localized corrosion and the formation of greigite and/or pyrite triggered by adjusting solution pH after 7 days of exposure. However, it was also possible that the localized corrosion occurred in Experimental set #2 was not related to the formation of greigite and/or pyrite but was due to the formation of elemental sulfur and/or polysulfides at high pH condition[8-11]. Therefore, one more experimental condition was designed and executed to better understand the mechanism for this type of localized corrosion in sour environments and confirm that it was indeed due to formation of greigite and/or pyrite. In the present experiment, the solution pH was adjusted after 2 days rather than 7 days as done in the previous experiment. The idea was that this was insufficient time for the development of a full mackinawite layer, which is a precursor for the transformation into more thermodynamically stable greigite and pyrite. In

this experiment, the formation of greigite and/or pyrite after the pH adjustment and the occurrence of localized corrosion were monitored.

Corrosion Behavior

Figure 13 shows pH values monitored during this experiment. The pH behavior of the present experiment was reproduced exactly the same as in the previous test Exp. set #2, but with the exception that solution pH was adjusted after 2 days of exposure.

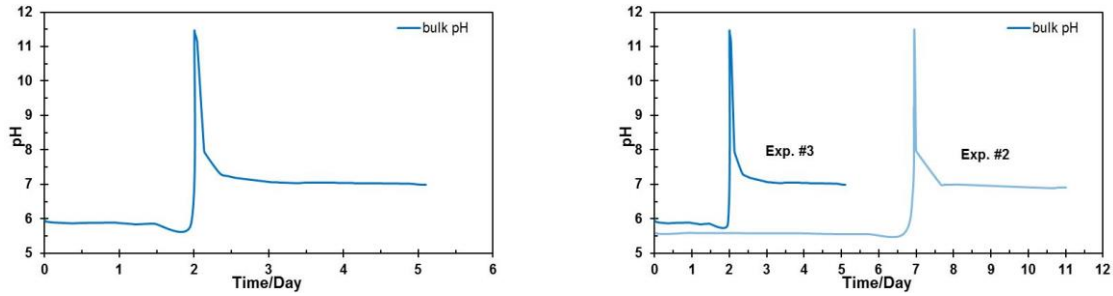

(a) (b)

Figure 13. (a) pH values monitored during Exp. #3; (b) comparison of pH values between Exp. #2 and Exp. #3.

Figure 14 shows OCP and corrosion rates monitored during the present experiment. A marked increase in the OCP after adjusting pH was observed, which is similar to Experimental set #2. However, the corrosion rate was stable throughout the experiment, which is different from Experiment set #2 that had an increased corrosion rate immediately after the pH adjustment.

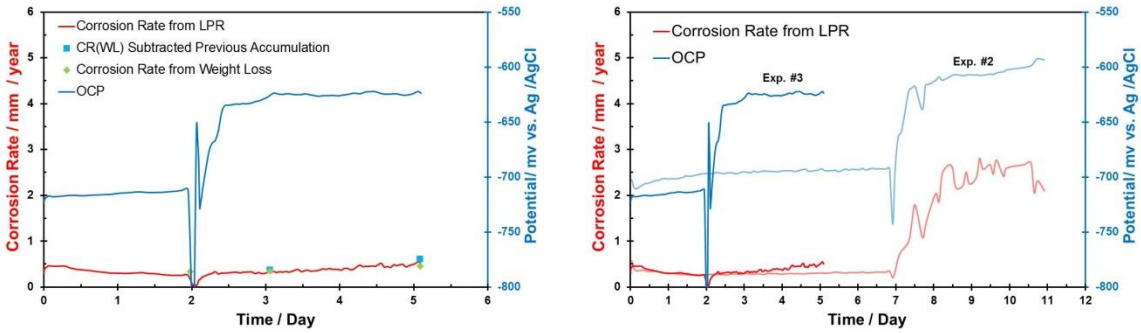

(a) (b)

Figure 14. (a) OCP and corrosion rate throughout experiment #3; (b) Comparisons of corrosion rate and OCP between Exp. #2 and Exp. #3.

Corrosion Products

Figure 15 shows surface morphologies of the specimen surface. Before the pH adjustment (after 1 day and after 2 days of test), a partially covered surface with corrosion product layer was observed on those samples. After the pH adjustment was performed, a uniform and fully covered corrosion product layer with lots of clusters on top of the layer was seen on the samples after 3 days and after 5 days of test, which is believed to be mackinawite precipitated at high pH conditions.

Table 5 presents XRD findings of corrosion products formed on those samples. For the samples before the pH adjustment, only mackinawite was detected. After the pH adjustment, a mixture of dominant mackinawite and pyrrhotite was observed. Neither greigite nor pyrite was detected after the pH adjustment. This is probably attributed to an insufficient time for the development of sufficient mackinawite, which is considered to be a precursor for transformation into greigite and pyrite.

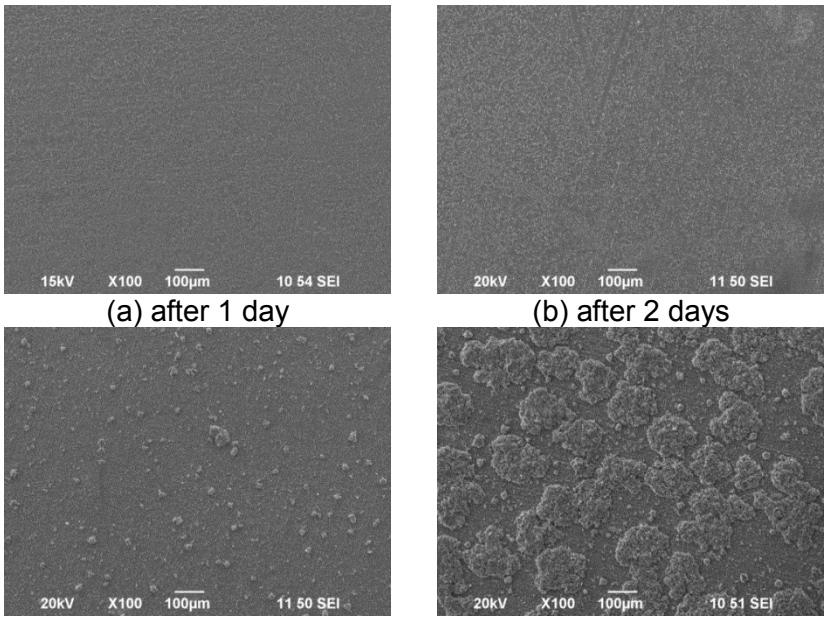

(a) after 1 day (b) after 2 days

(c) after 3 days (d) after 5 days

Figure 15. Surface morphologies of samples: (a) after 1 day; (b) after 2 days; (c) after 3 days; (d) after 5 days.

Table 5 XRD quantitative analysis of corrosion products formed in experiment #3.

Phases	2 days	3 days	5 days
Mackinawite	100 %	93.8 %	89.1 %
Pyrrhotite	0	2.1 %	7.3 %
Greigite	0	0	0
Pyrite	0	0	0
Iron Carbide	0	4.1 %	3.6 %

Surface Profilometry of Samples after Removing Corrosion Product Layer

The corrosion product layer was removed to check if localized corrosion occurred in the present experiment, particularly after the pH adjustment. A relatively flat surface indicating uniform corrosion before the pH adjustment was seen in Figure 16 (a). After the pH adjustment, a flat surface was observed on the sample after 3 days of exposure in Figure 16 (b) and also on the sample after 5 days of test in Figure 16 (c). Based upon the profilometry of these samples before and after pH adjustment, localized corrosion did not occur in the present experiment. This result confirms the fact that the localized corrosion observed in Exp. set #2 was not due to elemental sulfur and/or polysulfides formation in the solution at the high pH conditions. Although high pH conditions were reproduced, it seems that the development of mackinawite was insufficient for transformation into greigite and/or pyrite. Given that neither greigite nor pyrite was detected after the pH adjustment, this is proof of a strong connection between localized corrosion and the formation of greigite and/or pyrite.

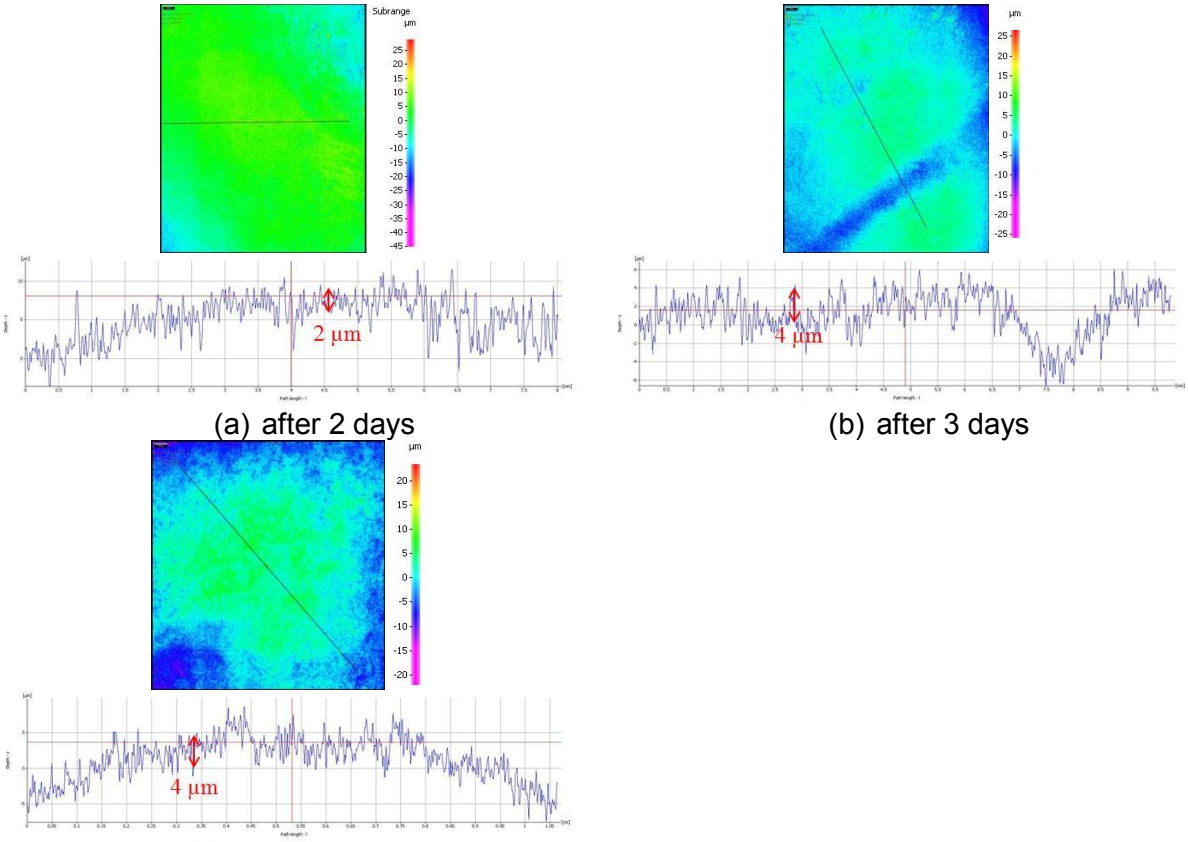

(a) after 2 days (b) after 3 days

(c) after 5 days

Figure 16. Surface profilometry of samples: (a) after 2 days; (b) after 3 days; (c) after 5 days.

SUMMARY

Based on these three sets of experiments, localized corrosion was observed only in conditions where there was formation of enough greigite and/or pyrite (including both spontaneous formation at high temperature and formation triggered by adjusting solution pH). Localized corrosion was not found when greigite and pyrite did not form. All of these experiments indicate that there is a strong correlation between the localized corrosion and the formation of greigite and/or pyrite. That is, formation of greigite and/or pyrite probably play an important role in the initiation of localized corrosion. However, the mechanism of this type of localization corrosion related to the formation of greigite and/or pyrite is not yet clear. It may be due to a galvanic effect related to difference in electrical conductivity associated with polymorphous iron sulfides[43-47] or it may be due to the local acidification at the steel sample surface[16] during the transformation process to greigite and/or pyrite.

CONCLUSIONS

- In the current experimental conditions, severe localized corrosion was observed in experiments when there was formation of greigite and/or pyrite. Localized corrosion was not found when neither greigite nor pyrite formed.
- The formation of greigite and/or pyrite plays an important role in the initiation of the localized corrosion.
- A further comprehensive study is required to investigate this correlation between localized corrosion and greigite and/or pyrite formation.

ACKOWLEDGEMENTS

The authors would like to express sincere appreciation to the following industrial sponsors for their financial support and direction: Anadarko, Baker Hughes, BP, Chevron, Clariant Oil Services, CNPC Tubular Goods, ConocoPhillips, DNV GL, Hess, INPEX Corporation, M-I SWACO, Multi-Chem, Nalco Champion, Occidental Oil Company, Petrobras, Petroleum Development Oman, Petroleum Institute (GRC), Petronas, PTT, Saudi Aramco, Sinopec, TransCanada, TOTAL, and Wood Group Integrity Management. The authors also appreciate the help offered at the Center for Electrochemical Engineering Research, Department of Chemical and Biomolecular Engineering at Ohio University, enabling the use of the XRD.

REERENCES

1. W. Sun, Ph.D. Dissertation, Ohio University, 2006.
2. B. Brown, Ph.D. Dissertation, Ohio University, 2013.
3. Y. Zheng, Ph.D. Dissertation, Ohio University, 2015.
4. D. W. Davis, R. A. Detro, “Fire and Brimstone The History of Melting Louisiana’s Sulphur”, Louisiana Geological Survey, Baton Rouge, Louisiana 1992.
5. D. D. MacDonald, B. Roberts, J. B. Hyne, “The Corrosion of Carbon Steel by Wet Elemental Sulphur”, Corros. Sci. 18, 5 (1978), pp. 411-425.
6. N. I. Dowling, P. D. Clark and J. B. Hyne, “Understanding and Mitigation Corrosion during Handling and Transportation of Elemental Sulfur”, Alberta Sulfur Research Center Quarterly Bulletin, Vol. XXXIII, No.1 April-June 1996, pp. 15-28.
7. N. I. Dowling, “Corrosion of Materials Used in Storage and Handling of Solid Elemental Sulphur”, Proceeding of the International Symposium on Materials Performance: Sulphur and Energy, 31st Annual Conference of Metallurgists of CIM, Edmonton, 1992, pp. 103-115.
8. H. Fang, “Investigation of Localized Corrosion of Carbon Steel in H_2S Environments,” Ph.D. dissertation, Dept. Chem. Eng, Ohio Univ., Athens, OH, 2011.
9. D. Precoor, “The detection, mitigation and corrosion mechanism of Ionic polysulfides in oil & gas systems,” CORROSION/2002.
10. J. Bojes, J. Lerbscher, W. Wamburi, and C. Dilley, “Elemenal sulfur in 3-phase sour gas systems-Is condensate really your ally?” NACE Northern Area Western Conference, Calgary, Alberta, February 2010.
11. A. Jr. Kamyshny, A. Goifman, J. Gun, D. Rizkov, and O. Lev, “Equilibrium distribution of polysulfide ions in aqueous solutions at 25oC: a new approach for the study of polysulfides’ equilibria,” *Environ. Sci. Technol.* 38, (2004): pp. 6633-6644.
12. D. F. Ho-Chung-Qui, A. I. Williamson, “Corrosion Experiences and Inhibition Practices in Wet Sour Gas Gathering Systems, Corrosion/1987, paper no. 46, 1987.
13. T. W. Hamby, “Development of high pressure sour gas technology”, Journal of Petroleum Technology, (1981): pp. 792-798.
14. H. Fang, B. Brown, S. Nesic, “High Salt Concentration Effects on CO2 Corrosion and H2S Corrosion,” Corrosion / 2010, paper no. 10276.
15. S. Nesic, Carbon Dioxide Corrosion of Mild Steel, in R. W. Revie, Ed., Uhlig’s Corrosion Handbook, 3rd ed., (Hoboken, NJ: John Wiley & Sons Inc., 2011) p. 229-245.
16. R. C. Woollam, A. Huggins, C. Mendez, J. R. Vera, W. H. Durnie, “Localized corrosion due to galvanic coupling between FeS-covered and uncovered areas: another oilfield myth?” Corrosion/2013, paper no. 2715, 2013.
17. J. Kvarekval, “Morphology of Localized Corrosion Attacks in Sour Environments,” Corrosion/2007, paper no. 07659 (Houston, TX: NACE, 2007).
18. W. Sun, S. Nesic, and S. Papavinasam, Corrosion 64, 7 (2008): p. 586-599.
19. E. Abelev, J. Sellberg, T. A. Ramanarayanan, S. L. Bernasek, *J. Mater. Sci.* 44, (2009): p. 6167-6181.
20. S. Kapusta, D. Raghu, J. Richard, Corrosion/2008, paper no. 08641, (Houston, TX: NACE, 2008).
21. Y. Zheng, J. Ning, B. Brown, D. Young, S. Nešić, “Mechanistic Study of the Effect of Iron Sulfide Layers on Hydrogen Sulfide Corrosion of Carbon Steel,” Corrosion/2015, paper no. 5933, 2015.
22. Y. Zheng, B. Brown, S. Nešić, Corrosion 70, 4 (2014): p. 351-365.

23. S. N. Smith, B. Brown, W. Sun, Corrosion/2011, Paper no. 11081 (Houston, TX: NACE, 2011).
24. B. Craig, “Corrosion product analysis- a road map to corrosion in oil and gas production,” Mater. Performance, August 2002, p. 56-58.
25. S. N. Smith, “Corrosion product analysis in oil and gas pipelines,” Mater. Performance, August 2013, p. 44-47.
26. K. Lee, Ph.D. Dissertation, Ohio University, 2004.
27. M. Singer, A. Camacho, B. Brown, S. Nesic, CORROSION/2010, paper no. 10100 (Houston, TX: NACE, 2010).
28. M. Singer, S. Nesic, J. N. Al-Khamis, CORROSION/2012, paper no. 0001411 (Houston, TX: NACE, 2012).
29. S. M. Wilhelm, “Galvanic corrosion caused by corrosion products,” in H. P. Hack, Ed., Galvanic Corrosion, ASTM STP 978, (American Society for Testing and Materials, Philadelphia, 1988) p. 23.
30. C. M. Menendez, V. Jovancicevic, S. Ramachandran, M. Morton, D. Stegmann, “Assessment of corrosion under iron sulfide deposits and CO2/H2S conditions,” *Corrosion* 69, 2 (2013): p. 145-156.
31. S. Standlee, K. D. Efird, D. Spiller, “Under deposit corrosion from iron sulfide,” Corrosion / 2011, paper no. 11266, 2011.
32. R. L. Martin, R. R. Annand, “Accelerated corrosion of steel by suspended iron sulfides in brine,” *Corrosion* 36, 5, (1981).
33. M. Achour, J. Kolts, P. Humble, R. Hudgins, “Experimental evaluation of corrosion inhibitor performance in presence of iron sulfide in CO2/H2S environment,” Corrosion / 2008, paper no. 08344, 2008.
34. J. Han, B. Brown, D. Young, S. Nesic, *J. Appl. Electrochem*., 40 (2010): p. 683-690.
35. J. Ning, Y. Zheng, D. Young, B. Brown, S. Nešić, “A Thermodynamic Model for the Prediction of Mild Steel Corrosion Products in an Aqueous Hydrogen Sulfide Environment,” *Corrosion* 71, 8 (2015): p. 945-960.
36. S. G. Clarke, “The Use of Inhibitors (with Special Reference to Antimony) in the Selective Removal of Metallic Coatings and Rust,” Trans. Electrochem. Soc. 69, 1 (1936): pp. 131-144.
37. ASTM G1 - 03 (2011), “Standard Practice for Preparing, Cleaning, and Evaluating Corrosion Test Specimens” (West Conshohocken,PA: ASTM).
38. D. W. Shoesmith, P. Taylor, M. G. Bailey, D. G. Owen, “The formation of ferrous monosulfide polymorphs during the corrosion of iron by aqueous hydrogen sulfide at 21 °C,” *J. Electrochem. Soc.* 127, 5 (1980): pp. 1007-1015.
39. Z. A. Iofa, V. V. Batrakov, Cho-Ngok-Ba, “Influence of anion adsorption on the action of inhibitors on the acid corrosion of iron and cobalt,” *Electrochimica Acta*, 9, 12, (1964): pp. 1645-1653.
40. D. R. Morris, L. P. Sampaleanu, D. N. Veysey, “The corrosion of steel by aqueous solutions of hydrogen sulfide,” *J. Electrochem. Soc.* 127, 6 (1980): pp. 1228-1235.
41. H. Ma, X. Cheng, G. Li, S. Chen, Z. Quan, S. Zhao, L. Niu, “The influence of hydrogen sulfide on corrosion of iron under different conditions,” *Corros. Sci.* 42, 10 (2000): pp. 1669-1683.
42. Y. Zheng, J. Ning, B. Brown, S. Nešić, “Electrochemical Model of Mild Steel Corrosion in a Mixed H2S/CO2 Aqueous Environment in the Absence of Protective Corrosion Product Layers,” *Corrosion* 71, 3 (2015): pp. 316-325.
43. A. J. Devey, “Computer Modeling Studies of Mackinawite, Greigite and Cubic FeS,” Ph.D. Dissertation, University College London, 2009.
44. C. Pearce, R. Pattrick, D. Vaughan, “Electrical and Magnetic Properties of Sulfides,” Sulfide Mineralogy and Geochemistry, Reviews in Mineralogy and Geochemistry, Mineralogical Society of America, 61 (2006): pp. 127-180.
45. R. Schieck, A. Hartmann, S. Fiechter, R. Konenkamp, H. Wetzel, “Electrical Properties of Natural and Synthetic Pyrite (FeS2) Crystals,” *J. Mater. Res.* 5, 7 (1990): pp. 1567-1572.
46. M. Caban-Acevedo, M. S. Faber, Y. Tan, R. J. Hamers, S. Jin, “Synthesis and Properties of Semiconducting Iron Pyrite (FeS2) Nanowires, ” *Nano Letters* 12, 4, (2012): pp. 1977–1982.
47. P. K. Abraitis, R. A. D. Pattrick, D. J. Vaughan, “Variations in the compositional, textural and electrical properties of natural pyrite: a review,” *Int. J. Miner Process* 74, (2004): pp. 41–59.